Engineering Injectable, Biocompatible, and Highly Elastic Bioadhesive Cryogels

Devyesh Rana¹, Thibault Colombani¹, Bahram Saleh¹, Halimatu Mohammad¹,

Nasim Annabi^{2,3,4,*}, Sidi A. Bencherif^{1,5,6,7,*}

¹Department of Chemical Engineering, Northeastern University, Boston, MA, USA.

²Harvard-MIT Division of Health Sciences and Technology, Massachusetts Institute of Technology, Cambridge, MA, USA

³Department of Chemical and Biomolecular Engineering, University of California, Los Angeles,
Los Angeles, CA, 90095, USA

⁴Center for Minimally Invasive Therapeutics (C-MIT), California NanoSystems Institute (CNSI),
 University of California, Los Angeles, Los Angeles, CA, 90095, USA
 ⁵Department of Bioengineering, Northeastern University, Boston, MA, USA
 ⁶Harvard John A. Paulson School of Engineering and Applied Sciences, Harvard University,
 Cambridge, USA

⁷Sorbonne University, UTC CNRS UMR 7338, Biomechanics and Bioengineering (BMBI), University of Technology of Compiègne, Compiègne, France

*Corresponding authors:

S. A. Bencherif, Email: s.bencherif@northeastern.edu

N. Annabi, Email: nannabi@ucla.edu

Abstract

The extracellular matrix (ECM), an integral component of all organs, is inherently tissue adhesive and plays a pivotal role in tissue regeneration and remodeling. However, man-made threedimensional (3D) biomaterials that are designed to mimic ECMs do not intrinsically adhere to moisture-rich environments and often lack an open macroporous architecture required for facilitating cellularization and integration with the host tissue post-implantation. Furthermore, most of these constructs usually entail invasive surgeries and potentially a risk of infection. To address these challenges, we recently engineered biomimetic and macroporous cryogel scaffolds that are syringe injectable while exhibiting unique physical properties, including strong bioadhesive properties to tissues and organs. These biomimetic catechol-containing cryogels were prepared from naturally-derived polymers such as gelatin and hyaluronic acid and were functionalized with mussel-inspired dopamine (DOPA) to impart bioadhesive properties. We found that using glutathione as an antioxidant and incorporating DOPA into cryogels via a PEG spacer arm led to the highest tissue adhesion and improved physical properties overall, whereas DOPA-free cryogels were weakly tissue adhesive. As shown by qualitative and quantitative adhesion tests, DOPA-containing cryogels were able to adhere strongly to several animal tissues and organs such as the heart, small intestine, lung, kidney, and skin. Furthermore, these unoxidized (i.e., browning-free) and bioadhesive cryogels showed negligible cytotoxicity toward murine fibroblasts and prevented the ex vivo activation of primary bone marrow-derived dendritic cells. Finally, in vivo data suggested good tissue integration and a minimal host inflammatory response when subcutaneously injected in rats. Collectively, these minimally invasive, browning-free, and strongly bioadhesive mussel-inspired cryogels show great promise for various biomedical applications, potentially in wound healing, tissue engineering, and regenerative medicine.

Keywords: biopolymers, dopamine, cryogel, bioadhesion, tissue adhesive

1. Introduction

Biomaterials, such as hydrogels, with bioadhesive properties are critical to various biomedical applications including tissue-engineered scaffolds to enhance their retention at the transplantation site and facilitate tissue integration. However, despite substantial advances in the design of bioadhesive hydrogels, wet tissue adhesion remains a significant challenge [1-3]. For instance, gelatin-based hydrogels offer good mechanical properties and biocompatibility but exhibit poor tissue adhesion. Fibrin-based hydrogels have also been investigated but also display limited tissue adhesion, poor tensile strength, and may cause a risk of blood-borne disease transmission and allergic reaction [4-7]. Additionally, most hydrogels require surgical implantation that can lead to several complications such as infection and damage to adjacent tissues [8]. Therefore, the need to engineer sophisticated and minimally invasive hydrogels has been at the forefront of material development especially for tissue engineering and regenerative medicine. To date, the design of a wet tissue adhesive hydrogel that can be delivered in a minimally invasive fashion while exhibiting suitable physical properties such as mechanical robustness and a macroporous network to facilitate tissue integration remains an unmet challenge.

Hydrogels with high water content fabricated from ECM-derived proteins such as gelatin and hyaluronic acid (HA) have been widely used in the biomedical field due to their intrinsic biological properties and similarity to native tissues [9-15]. However, these gels typically possess a mesoporous network, preventing suitable cellular infiltration, neovascularization, and ultimately tissue formation or integration [16]. Cryogels, a type of hydrogel with a set of unique physical features such as syringe-injectability and macroporous architecture (i.e., pores ≥10 um), have been gaining increasing interest in tissue engineering [17-30]. However, most injectable cryogels that have been engineered thus far do not exhibit strong bioadhesive and cohesive properties [31],

which may impact their overall performance and utility. For instance, strong tissue adhesion would be required for the design of cryogel-based patches to repair internal organs, especially dynamic organs (e.g., heart) undergoing large and repetitive volumetric deformations, or external organs such as the skin.

To impart hydrogels with bioadhesive properties, mussel-inspired dopamine (DOPA) and its polymerized version, polydopamine (PDA), have been extensively investigated [32, 33]. However, the catechol side chain of DOPA is susceptible to oxidation to form a quinone, which exhibits no adhesive properties and can decrease or even eliminate the strong interfacial bonds of the resulting DOPA-containing biomaterials with biological substrates [33]. Since DOPA and PDA adhere to humid surfaces, they have been incorporated into a variety of functional biopolymers, including gelatin and HA. However, when DOPA is oxidized, dark and potentially cytotoxic pigments are formed at high concentrations. As we previously reported, this oxidation mechanism could be prevented when a powerful antioxidative agent such as glutathione (GSH) is used [34].

In this work, we engineered minimally invasive, biomimetic, and macroporous mussel-inspired catechol-containing cryogel scaffolds via free radical polymerization at subzero temperature. These cryogels were prepared from gelatin or HA and were copolymerized with mussel-inspired DOPA derivatives to impart tunable bioadhesive properties. Both acrylated-DOPA (AD) and acrylated-polyethylene glycol DOPA (APD) were investigated as comonomers. We hypothesized that incorporating a spacer arm to DOPA when covalently anchored to the cryogel would enhance DOPA flexibility and eventually reinforce its bioadhesive strength to biological surfaces, specifically tissues and organs. Furthermore, we postulated that incorporating GSH could prevent DOPA oxidation, leading to increased bioadhesion while retaining the cryogels

colorless (i.e., no black-to-dark brown pigments as a result of the oxidative polymerization of DOPA to PDA). Next, we evaluated the physical properties of DOPA-containing cryogels such as injectability through a hypodermic needle, mechanical strength, and microporosity. Additionally, we qualitatively and quantitatively tested their bioadhesion to animal tissues and organs and assessed their cytocompatibility and cell-matrix interactions with murine fibroblasts (NIH 3T3). The *in vitro* biocompatibility of DOPA-containing cryogels was examined with primary bone marrow-derived dendritic cells (BMDCs). Lastly, we assessed their tissue integration and host immune response when subcutaneously injected in mice.

2. Methods

2.1 Materials. DOPA, GSH, HA, gelatin, methacrylic anhydride (MA), glycidyl methacrylate (GM), acrylic acid N-hydroxysuccinimide ester (ACRL-NHS), dimethylformamide (DMF), Dulbecco's phosphate-buffered saline (PBS), DPX mounting medium, hematoxylin and eosin (H&E) staining kit, triethylamine, sodium bicarbonate (NaHCO3), tetramethylethylenediamine (TEMED), and ammonium persulfate (APS) were purchased from MilliporeSigma (Burlington, MA) and used without any further purification. Acrylate-PEG-succinimidyl valerate (ACRL-PEG-NHS, MW 3400) was obtained from Laysan Bio Inc. (Arab, AL). Ethyl 2-cyanoacrylate glue (Krazy glue, Westerville, OH) was purchased from the local hardware store. Dulbecco's Modified Eagle Medium (DMEM, Gibco), fetal bovine serum (FBS), and penicillin/streptomycin (Pen-Strep) were purchased from Thermo Fisher Scientific Inc. (Waltham, MA). Calcein AM/ethidium homodimer-1 live/dead kit was purchased from Genecopeia. Fluorescent antibodies MHC II (M5/114.15.2, Rat IgG2b, PE/Cy7), CD86 (GL1, rat IgG2a, PE), CD11c (N418, hamster IgG,

APC), and CD11b (M1/70, rat IgG2b, κ, APC) were purchased from Biolegend Inc. (San Diego, CA). CD45 (rabbit IgG), Mannose Receptor/CD206 (rabbit IgG) and anti-F4/80 (rabbit IgG) were purchased from Abcam Inc. (Waltham, MA). Goat anti-rabbit (IgG) Alexa Fluor 594-conjugated secondary antibody was obtained from Invitrogen Inc. (Waltham, MA).

- 2.2 Functionalization of DOPA. To synthesize ACRL-DOPA (AD) or ACRL-PEG-DOPA (APD), vials sealed with rubber caps and containing 2.5 mg of GSH were dissolved in 5 mL of NaHCO₃ buffer (pH 8.5) and subsequently flushed with nitrogen for 30 min to remove air. Next, DOPA and ACRL-NHS (for AD) or DOPA and ACRL-PEG-NHS (for APD) were quickly added at a 1:1 molar ratio and nitrogen was flushed again for another 30 min. The reaction vessels were then placed on a shaker plate to allow the reactions to proceed overnight. The following day, the samples were frozen at -20 °C and subsequently lyophilized to obtain the final products: AD or APD.
- **2.3 Functionalization of HA and gelatin.** Methacrylated HA (HAGM) and methacrylated gelatin (GelMA) were synthesized as previously described [9, 35-37]. Briefly, for the preparation of HAGM, a total of 1 g of HA was dissolved in 200 mL PBS (pH 7.4) and subsequently mixed with 67 mL of DMF, 13.3 g of GM, and 6.7 g of triethylamine. After 10 days of reaction, the solution was precipitated in an excess of acetone, filtered, and dried overnight in a vacuum oven. HAGM was then used without any further processing. Similarly, for the preparation of GelMA, type A porcine skin gelatin dissolved at 10% (w/v) concentration in PBS at 60 °C and stirred until fully dissolved. A total of 10 g of MA was added dropwise under stirred conditions at 50 °C and allowed to react for 1 h. Following a 1:5 dilution with additional warm (40 °C) PBS to stop the reaction, the mixture was dialyzed against diH₂O using 12–14 kDa cutoff dialysis tubing for 1 week at 40 °C

to remove impurities (i.e., salts and unreacted MA). Finally, GelMA was lyophilized for 1 week to generate a white foam solid and stored at -80 °C until further use.

2.4 Preparation of HAGM and GelMA-based bioadhesive cryogels. HAGM or GelMA were used as is or combined with AD or APD to fabricate HAGM-co-AD (HD) and HAGM-co-APD (HPD) or GelMA-co-AD (GD) and GelMA-co-APD cryogels (GPD), respectively. To initiate the cryopolymerization process, 0.1% (w/v) TEMED, and 0.5% (w/v) APS were added to the precursor solutions immediately prior to use. The polymer precursor solutions were then pipetted into preformed cubical (4 x 4 x 1 or 10 x 5 x 1 mm³) or cylindrical (height x diameter: 6 x 8 mm² or 10 x 1 mm²) Teflon molds. Next, the molds were immediately placed in a freezer at -20 °C for 16 h to allow cryopolymerization. Finally, cryogels were thawed at room temperature, removed from the molds, washed in PBS, and immediately used for all subsequent experiments.

2.5 Characterization of polymers and cryogels by ¹H NMR. Proton nuclear magnetic resonance (¹H NMR) analysis was conducted to evaluate the degree of methacrylation of HAGM and GelMA and assess qualitatively their vinyl group consumption following cryogelation using a Varian Inova-500 NMR spectrometer. Deuterium oxide (D₂O) was used as solvent, and the concentration of the modified polymers was kept at 1% (w/v). For chemical characterization of the cryogels, cryogelation was induced directly in an NMR tube. One milliliter of the prepolymer solution containing the initiator system (APS/TEMED) was transferred into the NMR tube before cryogenic treatment at -20°C for 16 h. All ¹H NMR spectra were obtained at room temperature, 15 Hz sample spinning, 45° tip angle for the observation pulse, and a 10 second recycle delay, for 128 scans. Peak values at 5.2 and 5.5 ppm for HAGM and at 5.4 and 5.7 ppm for GelMA were correlated to the presence of methacrylated groups. Peak areas were integrated using

ACD/Spectrus NMR analysis software and degrees of methacrylation for each polymer type were determined as previously described [9, 37, 38].

2.6 Adhesion properties of bioadhesive cryogels. To assess tissue adhesion, the wound closure strength of DOPA-free and DOPA-containing cryogels on porcine skins was determined using the American Society for Testing and Materials (ASTM) F2458-05 standard test method [39]. A fresh porcine skin was obtained from a local butcher shop and cut into small fat-free strips (1×2 cm²). Tissues were immersed into PBS before testing to prevent drying in the air. The tissues were fixed onto two pre-cut poly(methyl methacrylate) slides (2×6 cm²) by ethyl 2-cyanoacrylate glue. Approximately 6-mm spaces were kept between the slides using the porcine skin. The tissue was then separated in the middle with a straight edge razor to simulate the wound. For each formulation, a cuboidal cryogel (dimensions: $10 \times 5 \times 1$ mm³) was placed onto the simulated wound site. Next, samples were then mounted onto an Instron 5542 Mechanical Tester and the entire construct was extended. Maximum adhesive strength of each sample was obtained at the point of tearing at strain rate of 1 mm/min (n = 5). Data were obtained and analyzed using the Instron's accompanying Bluehill 3 software.

The burst pressure of DOPA-free and DOPA-containing cryogels was calculated by using the ASTM F2392-04 standard test method [40]. Evicel® and CoSeal®, two clinically available surgical sealants were used for comparison. Freshly harvested porcine intestine tissues were obtained from a local butcher. The intestine tissues were placed between two stainless steel annuli from a custom-built burst-pressure apparatus, consisting of a metallic base holder, pressure meter, syringe pressure setup, and data collector. A pin-sized hole puncture was made through the intestine tissues and air was flowed using a syringe pump at 0.5 ml/s. The hole made on the intestine was covered with a preformed cylindrical cryogel (height x diameter: 1 x 20 mm²) prior

to initiating the pump and sensor. Airflow was terminated post cryogel rupture and the burst strength (pressure) was recorded (n = 5).

2.7 Mechanical properties of bioadhesive cryogels. Cryogels were first incubated for 1 h in PBS and their dimensions were measured using a digital caliper. Uniaxial tensile and cyclic uniaxial compression tests were conducted using an Instron mechanical tester. Cryogels for tensile testing were placed between two pieces of double-sided tape within the tension grips of the instrument and extended at a rate of 1 mm/min until failure. Elastic moduli were calculated by obtaining the slope of the stress-strain curves. Cryogels for compressive testing were loaded onto compression plates of the instrument under wet conditions, by submerging the plates in PBS. Cyclic uniaxial compression tests were conducted at a 90% strain level and 1 mm/min strain rate. Cryogels were conditioned cyclically (loading and unloading) for 7 cycles. Post-conditioning, the cryogel underwent a final cycle. Compressive strain (mm) and load (N) were then measured at the 8th cycle using the Instron's Bluehill 3 software. Moduli were determined by obtaining the tangent of the slope of the linear region on the loading stress/strain curve. Energy loss was calculated by obtaining the area between the loading and unloading curves (n = 5).

The swelling ratio was determined using a conventional gravimetric procedure. Cylindrical cryogels (height x diameter: 6 x 8 mm²) were prepared and immersed in PBS for 24 h prior to the experiment. The equilibrated mass swelling ratio (Q_M) was calculated by dividing the mass of fully swollen by the mass of freeze-dried cryogel. The cryogels were washed in diH₂O for salt removal prior to being freeze-dried.

To quantify the degrees of pore connectivity, fully hydrated cryogels were first weighed on an analytical scale. Next, a Kimwipe was lightly applied to the scaffolds' surfaces to wick away free water. The weight of partially dehydrated cryogels was recorded again. The degree of pore

connectivity was calculated based on the weight of water wicked away divided by the initial weight of hydrated cryogels.

To determine the pore size and pore size distribution by scanning electron microscopy, freeze-dried cryogels (4 x 4 x 1 mm³) were mounted on the sample holder using carbon tape and sputter-coated with platinum/palladium up to 5 nm of thickness. Samples were then imaged using secondary electron detection on a Hitachi S-4800 scanning electron microscope (Hitachi High-Technology Corporation, Tokyo, Japan) while operating at 3 kV and 10 mA. Pore sizes were quantified by measuring pore diameters using ImageJ.

- **2.8 Two-dimensional (2D) cell seeding.** NIH 3T3 fibroblast cells were cultured in DMEM supplemented with 10% FBS and 1% Pen-Strep. For 2D cell culture, 4% (w/v) cuboidal cryogels (4 x 4 x 1 mm³) were used. Cells were seeded on cryogels at a concentration of 2 x 10⁶ cells/mL and subsequently incubated in a humidified atmosphere containing 5% CO₂ at 37 °C.
- **2.9 Cell viability and proliferation assay.** Cell viability was determined using a Calcein AM/ethidium homodimer-1 live/dead kit according to the manufacturer's instructions. The experiments were performed one day post-seeding. Fluorescence images were acquired using a Zeiss Axio Observer Z1 inverted microscope and analyzed using ImageJ software. Cell viability was determined as the ratio of viable cells to the total number of cells.
- **2.10** Generation and *in vitro* activation assay of bone marrow-derived dendritic cells (BMDCs). Eight-week-old C57BL/6 mice (The Jackson Laboratory, Bar Harbor, ME) were housed in conventional conditions according to NIH guidelines. All animal experiments were performed in accordance with NIH recommendations and approved by the Division of Laboratory

Animal Medicine (DLAM) at Northeastern University. BMDCs were extracted from C57BL/6 femur bone marrow as previously described [23, 41], then cultured for 6 days in Roswell Park Memorial Institute medium (RPMI 1640, Fisher Scientific) supplemented with 10% heatinactivated FBS, 100 U/mL penicillin, 100 μg/mL streptomycin, and 20 ng/mL murine GM-CSF (Genscript, Piscataway, NJ). To evaluate BMDC activation induced by different types of cryogels, cuboidal cryogels (4 x 4 x 1 mm³) were incubated with BMDCs for 1 day in RPMI 1640 supplemented with 10% FBS and 1% penicillin-streptomycin. BMDCs maturation was then evaluated by flow cytometry (BD FACSCalibur DxP upgraded, Cytek Bioscience, Fremont, CA) using the following fluorescent antibodies (Biolegend, San Diego, CA): MHC II (M5/114.15.2, Rat IgG2b, PE/Cy7), CD86 (GL1, rat IgG2a, PE), CD11c (N418, hamster IgG, APC), and CD11b (M1/70, rat IgG2b, κ, APC). Negative and positive controls consisted of BMDCs cultured in media alone and media supplemented with 100 ng/mL of lipopolysaccharide (LPS), respectively.

2.11 *In vivo* subcutaneous implantation of cryogels. All animal experiments were reviewed and approved by Institutional Animal Care and Use Committee (ICAUC, protocol 15–1248R) at Northeastern University. Male Wistar rats (200–250 g) were obtained from Charles River (Boston, MA) and housed in the local animal care facility under conditions of circadian day–night rhythm and *ad libitum* feeding. Anesthesia was induced by 2.5% isoflurane inhalation, followed by SC buprenorphine (0.02–0.05 mg/kg) administration. Next, cuboidal 4% (w/v) HAGM cryogels (dimensions: 4 x 4 x 1 mm³) were subcutaneously injected using a sterile 16-gauge hypodermic needle.

Prior to injection, the cryogels were disinfected in 70% ethanol (v/v) for 20 min and subsequently sterilized under UV germicidal irradiation for 60 min a wavelength of 254 nm. Cryogels (suspended in 0.2 mL of PBS) were loaded into sterile hypodermic 16G needles and

subsequently injected using a 1-mL syringe into subcutaneous pockets along the dorsomedial skin of male Wistar rats. After 21 days post-implantation, animals were euthanized and the cryogels were retrieved along with the surrounding tissues for histological assessment. Explants were thoroughly washed in diH₂O, and excess tissue was carefully removed under a dissection microscope.

- 2.12 Histological analysis and immunofluorescent staining. Following explantation, samples were fixed in 4% (v/v) paraformaldehyde for 4 h, followed by overnight incubation in 30% (w/v) sucrose at 4 °C. Samples were then embedded in OCT and flash-frozen in liquid nitrogen. Frozen samples were sectioned using a Leica Biosystems CM3050 S Research Cryostat. Cryosections (14-µm thick) were obtained and mounted on positively charged slides using DPX mounting medium. Slides were then processed with H&E staining according to the manufacturer's instructions. Immunohistofluorescent staining was performed on mounted cryosections as previously reported [42]. Anti-CD45 (Abcam, rabbit IgG), anti-Mannose Receptor/CD206 (Abcam, rabbit IgG), and anti-F4/80 (Abcam, rabbit IgG) were used as primary antibodies, and goat anti-rabbit (IgG) Alexa Fluor 594-conjugated secondary antibody (Invitrogen) was used for detection. All sections were counterstained with DAPI (Invitrogen) and imaged on an AxioObserver Z1 inverted microscope.
- **2.13 Statistical Analysis.** All values were expressed as mean \pm standard deviation (SD). Statistical analyses were performed using GraphPad Prism Software (La Jolla, CA). Significant differences between groups were analyzed by one-way analysis of variance (ANOVA). Differences were considered significant at *p < 0.05, **p < 0.01, ***p < 0.001, ****p < 0.0001.

3. Results

3.1 Fabrication and characterization of bioadhesive cryogels. Biomimetic and syringe-injectable cryogels were prepared from gelatin and HA and were functionalized with DOPA, a mussel-inspired catechol-based strategy to impart wet adhesive properties that mimic mussel adhesive protein glues.

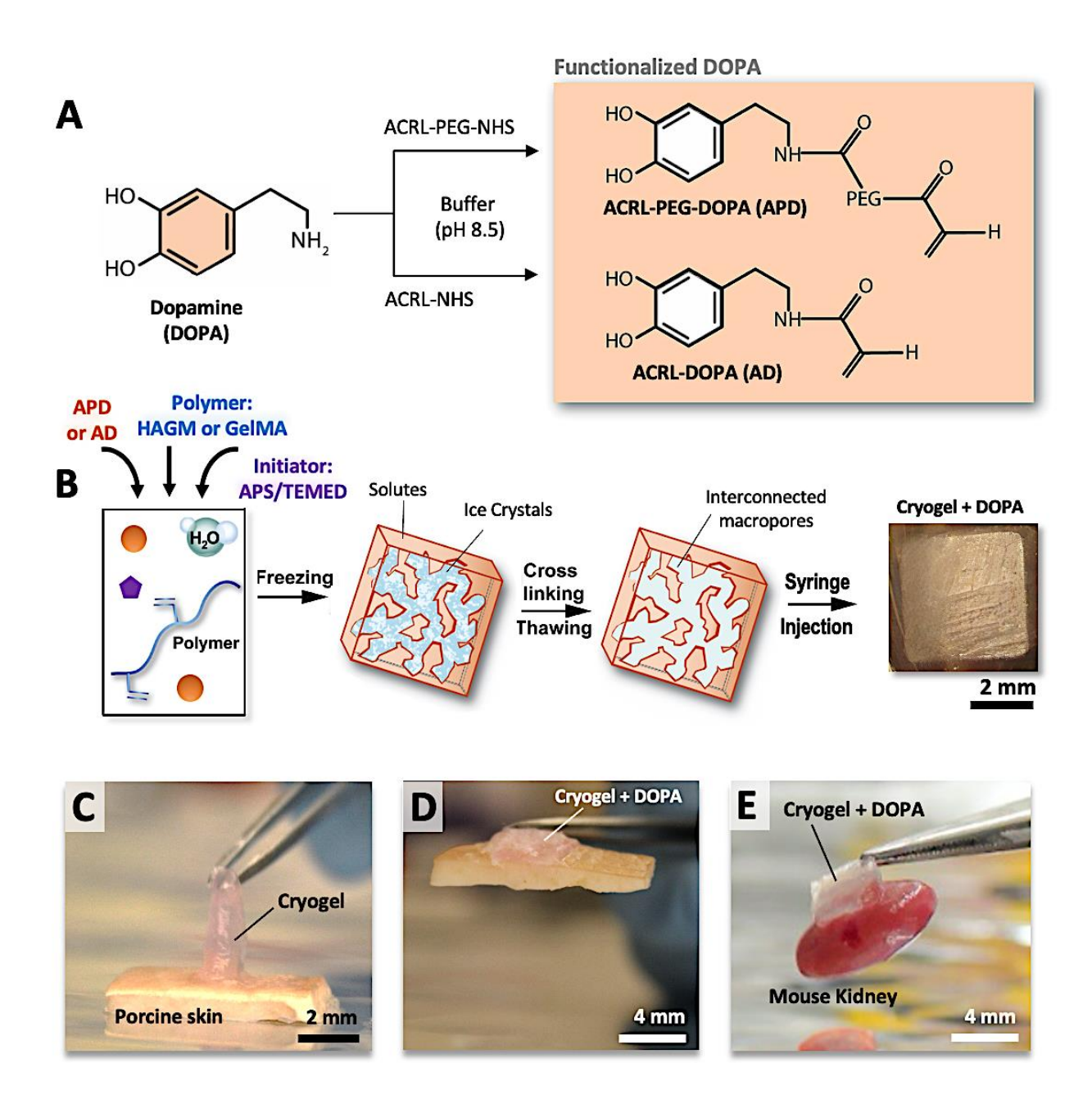


Figure 1. Schematic depicting DOPA functionalization and fabrication of minimally invasive bioadhesive cryogels. (**A**) Functionalization of DOPA with either acrylic acid N-hydroxysuccinimide ester (ACRL-NHS) or NHS-activated PEG-acrylate (ACRL-PEG-NHS) to form ACRL-DOPA (AD) and ACRL-PEG-DOPA (APD), respectively. (**B**) Illustration displaying the process of cryogelation. An aqueous solution containing functionalized DOPA (AD or APD), polymerizable biopolymers (HAGM or GelMA), and an initiator system (APS and TEMED) is incubated overnight at –20 °C. Cryogelation is a process in which gelation occurs under semi-frozen conditions via several steps: phase separation with ice-crystal formation, crosslinking, and thawing of ice-crystals to ultimately form interconnected porous and injectable bioadhesive cryogels. Photographs depicting the bioadhesive properties of DOPA-free (**C**) and DOPA-containing (**D**) cryogels on porcine skin tissues and DOPA-containing cryogels on a mouse kidney (**E**).

To prepare DOPA amenable to cryogelation, pendant acryloyl groups were first introduced into the reagent. DOPA was functionalized with ACRL-NHS to yield polymerizable AD (**Fig 1A**). Additionally, to reduce the steric hindrance and optimize spatial arrangement, DOPA was also functionalized with ACRL-PEG-NHS to yield polymerizable APD. The rationale of using a hydrophilic PEG spacer arm is to give DOPA a long and flexible connection to minimize steric hindrance, ultimately increasing the likelihood of binding to tissues and as a result, achieving improved bioadhesion. To prepare HA and gelatin amenable to polymerization, these biopolymers were methacrylated as previously described [9, 43]. As depicted in **Fig 1B**, bioadhesive cryogels were prepared by the process of cryogelation at -20 °C using an aqueous prepolymer solution containing methacrylated HA (HAGM) or methacrylated gelatin (GelMA), AD or APD, and the initiator system. **Figs S1** and **S2** confirmed that the vinylic peaks disappeared after cryopolymerization across all formulations (HD, HPD, GD, and GPD), suggesting total consumption of the reactive pendant methacrylate and acrylate groups. As a result, unlike standard

(DOPA-free) cryogels, DOPA-containing cryogels are endowed with strong wet adhesion properties on animal-derived tissues such as porcine skin and mouse kidney (**Fig 1C–E**).

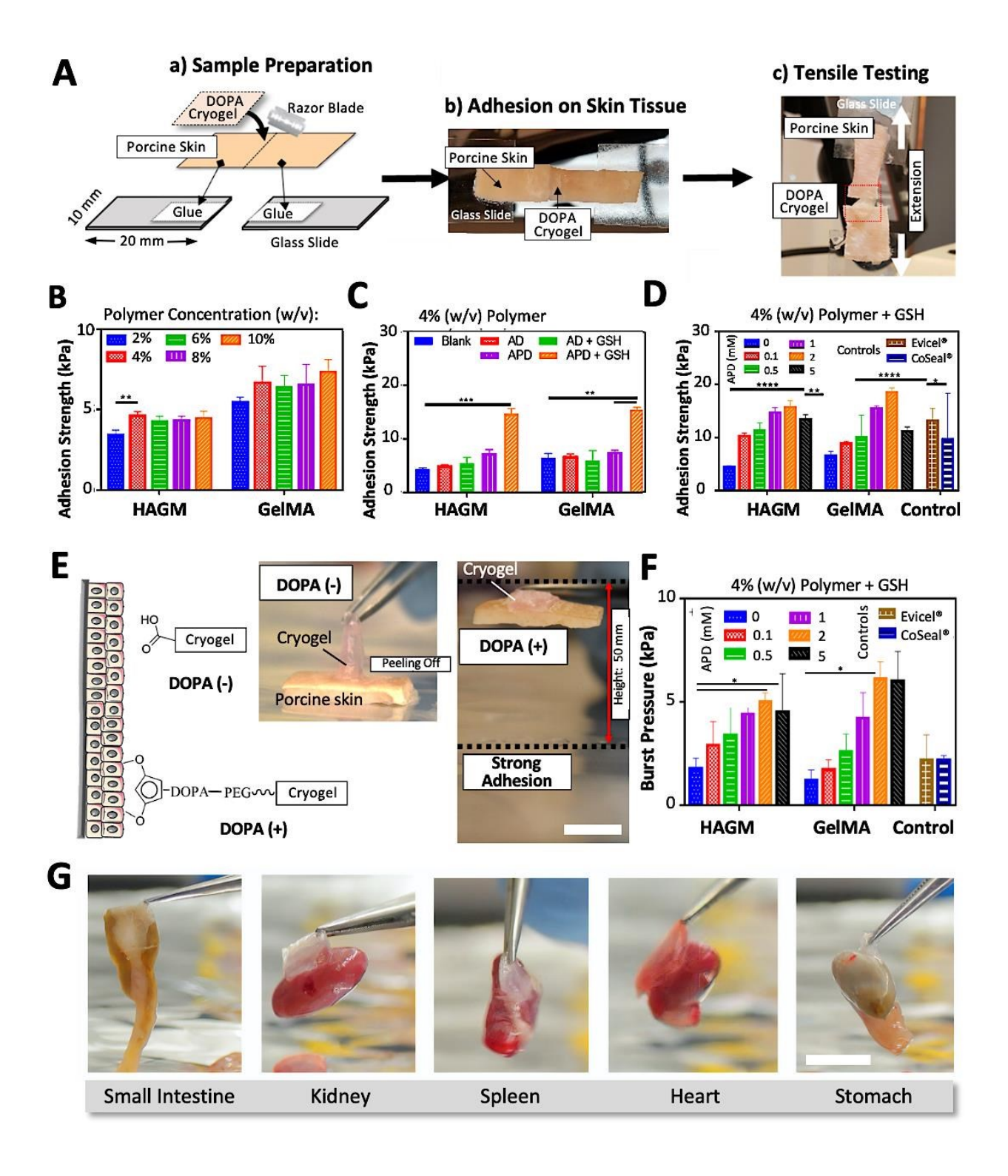


Figure 2. Adhesion properties of DOPA-containing cryogels. (A) Schematic illustration depicting sample preparation and wound closure testing to characterize the tensile strength of DOPA-containing cryogels as a topical adhesive on porcine skin tissues. A tensile tester was used to pull the samples apart and record each wound closure maximum disruption forces (i.e., adhesion strengths). Adhesion strength measurements of DOPA-free HAGM and GelMA-based cryogels as a function of polymer concentration (B) and DOPA (i.e., AD or APD)-containing HAGM and GelMA-based cryogels supplemented without (C) and with (D) GSH. (E) Left: overview of the adhesive interactions between the catechol group and biological tissues. Right: illustration depicting an adhesive peal test. (F) Adhesion burst measurements of GSH-supplemented DOPA-containing HAGM and GelMA-based cryogels. (G) Photographs depicting the strong bioadhesive strengths of DOPA-containing cryogels across various adult mouse internal organs (small intestine, kidney, spleen, heart, and stomach) when picked up with a tweezer. Scale bars = 1 cm. Values represent the mean ± SD and data were analyzed using one-way ANOVA (n = 5). *p < 0.05, **p < 0.01, ***p < 0.001, and ****p < 0.001, and ****p < 0.0001.

3.2. *In vitro* **adhesion testing of DOPA-containing cryogels.** Standard wound closure and burst pressure tests were performed across various cryogels. ASTM F2458-05, a commonly used standard test for measuring wound closure strength of tissue adhesives [39], was used to evaluate the adhesion properties of HAGM (DOPA-free, control), DOPA-containing HAGM (HD, HPD), GelMA (DOPA-free, control), and DOPA-containing GelMA (GD, GPD) cryogels. Furthermore, the bioadhesive properties of cryogels were compared to Evicel® and CoSeal®, two commercially available and widely used sealants in the clinic.

As shown in **Fig 2A**, wound closure tests, a technique used to reproduce pulling or stretching forces, were performed to determine the adhesive strength of the engineered cryogels on animal tissues (i.e., freshly harvested porcine skin) according to the ASTM standard. The

adhesive strength of DOPA-free HAGM or GelMA cryogels remained relatively low and relatively constant regardless of the polymer concentration (**Fig 2B**). Specifically, 2 to 10% HAGM and GelMA cryogels displayed statistically non-significant adhesion properties varying between 3.4 ± 0.3 to 4.5 ± 0.4 kPa and 5.5 ± 0.3 to 7.3 ± 0.8 kPa, respectively. This data set was expected due to the lack of catechol side chains from DOPA, crucial moieties known to play a synergetic effect for adhesion to substrates of widely varying composition from inorganic to organic [44]. A polymer concentration of 4% (w/v) was chosen due to its superior handleability and processability (i.e., lower viscosity), although a higher polymer concentration (i.e., 10%) resulted in DOPA-free GelMA-based cryogels with a slightly higher bioadhesion strength.

Next, we evaluated the incorporation of DOPA into 4% (w/v) cryogels (AD and APD) and its effect on tissue adhesion with and without the presence of GSH. The tripeptide (cysteine, glycine, and glutamic acid), a naturally occurring and powerful antioxidant, was used to mitigate overoxidation and maintain enough free catechol groups during DOPA functionalization, polymerization/cryogelation, and the adhesion process [33]. DOPA is susceptible to oxidation to form quinones, potentially leading to weak and unstable bioadhesion of catechol moieties.

As depicted in **Fig 2C**, the adhesion strengths of cryogels, namely HD (4% HAGM + 1 mM AD) and HPD (4% HAGM + 1 mM APD) were 5.3 ± 0.2 kPa and 7.3 ± 0.7 kPa, respectively, compared to 4.4 ± 0.2 kPa for DOPA-free HAGM (control). Similarly, the adhesion strengths of GD (4% GelMA + 1 mM AD) and GPD (4% GelMA + 1 mM APD) cryogels were 6.8 ± 0.5 kPa and 7.6 ± 0.3 kPa, respectively, compared to 6.5 ± 0.8 kPa for DOPA-free GelMA cryogels (control). As we previously reported, GSH reduces DOPA oxidation [34], potentially improving adhesion properties while preventing oxidative browning (**Fig S3**). Therefore, with the addition of GSH, increased adhesion strengths were achieved for all DOPA-containing formulations,

especially for cryogels formulated with APD. Specifically, HD, HPD, GD, and GPD cryogels exhibited adhesion strengths of 5.5 ± 1.1 kPa, 14.7 ± 0.98 kPa, 6.1 ± 1.8 kPa, and 15.5 ± 0.4 kPa, respectively. Compared to HD and GD, the significant increase in adhesion strengths for HPD and GPD is likely due to the introduction of a PEG spacer arm, minimizing the steric hindrance of DOPA and ultimately increasing binding to tissues. Accordingly, APD was preferred for the formulation of bioadhesive cryogels. Our third optimization was based on varying the ratio of the highest adhesion strength yielding polymer formulations (HPD and GPD) with GSH to fine-tune the amount of APD required for reaching maximum bioadhesion forces. APD at 2 mM resulted in the highest adhesion strengths when formulated with HAGM or GelMA (Fig 2D). Specifically, HPD and GPD (4% polymer + 2 mM APD) cryogels displayed adhesion strengths of 15.7 \pm 1.2 kPa and 18.5 ± 0.8 kPa, respectively. Surprisingly, at higher concentrations (>2 mM), APD led to decreased adhesion strength. For instance, at 5 mM APD, the adhesion strength for HPD and GPD dropped to 13.4 ± 0.8 kPa and 11.2 ± 0.8 kPa, respectively. Our results further showed that our bioadhesive cryogels displayed either higher or similar adhesion properties when compared to commercially available surgical adhesives such as Evicel[®] (13.2 \pm 2.3 kPa) and CoSeal[®] (9.6 \pm 8.7 kPa). Therefore, concentrations of 4% (w/v) polymer and 2 mM APD were selected for subsequent studies. In addition, in vitro burst pressure testing based on the ASTM F2392-04 standard was performed using a wet collagen sheet to determine the ability of the engineered cryogels to seal tissues under air or liquid pressures. An illustration depicting the adhesive peal test is shown in Fig 2E. The burst pressure of APD (up to 5 mM)-containing HAGM and GelMA cryogels resulted in a similar trend to the wound closure data (Figs 2F and S4). Specifically, HPD and GPD (formulated with 2 mM APD) displayed a burst pressure of 5.0 ± 0.4 kPa and 6.1 ± 0.8 kPa, respectively.

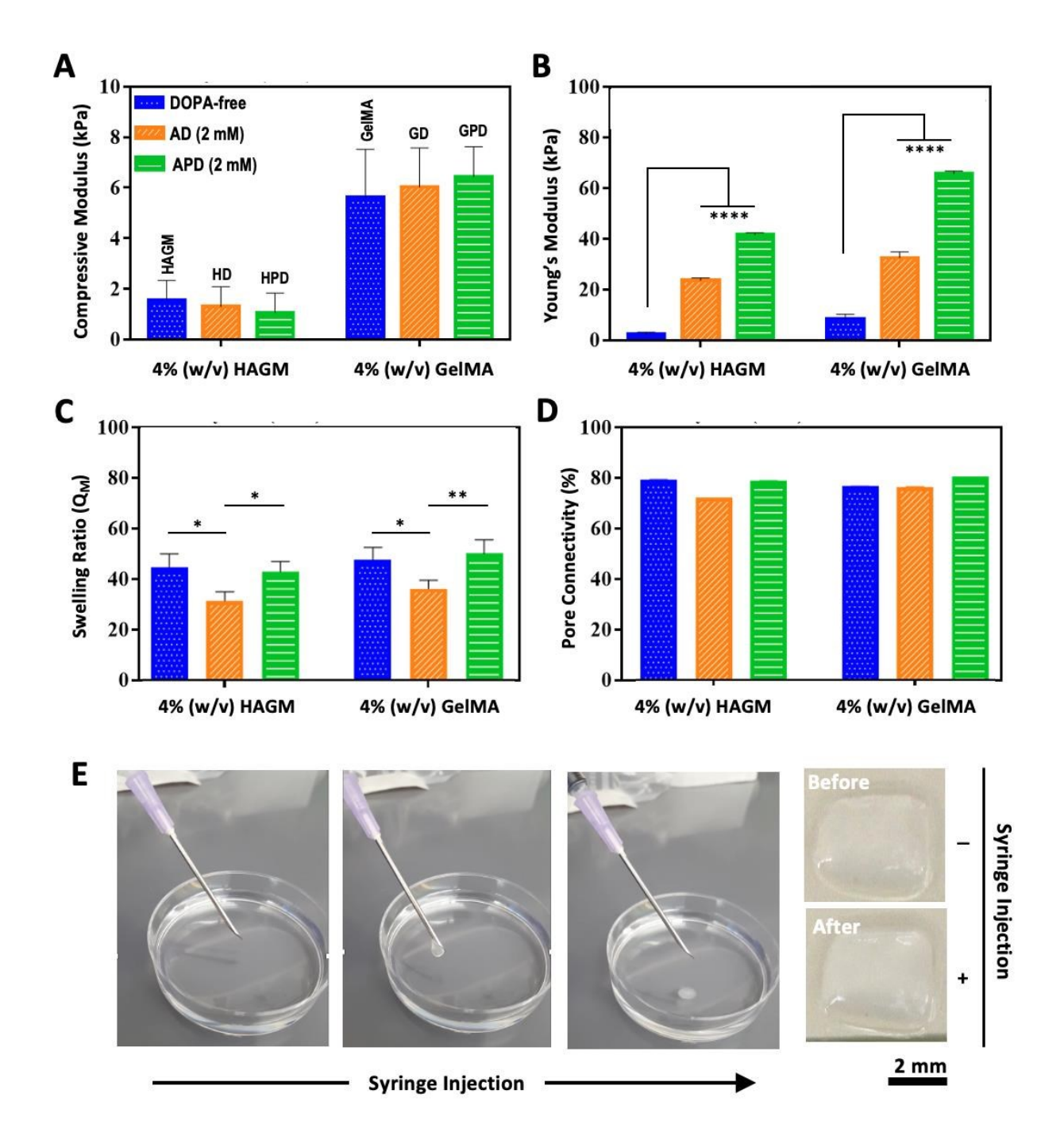


Figure 3. Physical characterization of bioadhesive cryogels. Compressive modulus (**A**), Young's modulus (**B**), swelling ratio (**C**), and degree of pore connectivity (**D**) of GSH-supplemented DOPA (i.e., AD or APD)-containing HAGM and GelMA-based cryogels. (**E**) Photographs depicting the successful syringe injection of bioadhesive cryogels using a 16-gauge hypodermic needle. HAGM: DOPA-free HAGM, GelMA: DOPA-free GelMA, HD: AD-containing HAGM, HPD (APD-containing HAGM), GD

(AD-containing GelMA), GPD (APD-containing GelMA). Values represent the mean \pm SD and data were analyzed using one-way ANOVA (n = 5). ****p < 0.0001.

Unlike HPD cryogels, GPD cryogels did not exhibit consistent burst pressure and adhesion strength behaviors. At 5 mM APD, the burst pressure for GelMA-based cryogels displayed a lower flexural strength compared to the adhesion strength, whereas the HAGM-based cryogels displayed a more consistent pattern. This may be due to the high concentration of ADP within GelMA-based cryogels, resulting in a more brittle construct.

Additionally, HPD and GPD cryogels containing 5 mM APD resulted in a slight decrease in burst pressures, 4.5 ± 1.8 kPa and 6.0 ± 1.4 kPa, respectively. Comparatively, Evicel® and CoSeal® resulted in lower burst pressures of 2.2 ± 1.2 kPa and 2.2 ± 0.2 kPa, respectively. Overall, HPD and GPD cryogels outperformed commercially available sealants, with increased burst pressure values up to 277%. Lastly, cuboidal (4 x 4 x 1 mm³) bioadhesive HPD cryogels (4% polymer + 2 mM APD) were tested for their ability to adhere to various adult mouse internal organs (small intestine, kidney, spleen, heart, and stomach) of different sizes and weights (**Fig 2G, Video S1**). Strikingly, DOPA-containing cryogels were able to adhere strongly to all organs, lifting up to 60 times their own weights (cryogel: ~17 mg, small intestine: ~1100 mg) [45].

Both properties, wound-bursting and wound closure strengths, are particularly beneficial for injectable tissue adhesives to fully adhere to tissue defect surfaces and improve tissue integration and eventually healing. As an example, these properties show the ability to withstand high pressures occasionally exerted on pulmonary tissue during invasive mechanical ventilation such as by recruitment maneuvers. In this scenario, pressure values can reach up to 40 cm H₂O of intra-alveolar peak pressure (3.9 kPa) [46], which is typically not attainable by commercially available products [47-49].

3.3. Physical characterization of bioadhesive cryogels. The physical properties of spacer-containing DOPA-containing cryogels, namely HPD and GPD, were evaluated and compared to spacer-free DOPA-containing (HD and GD) and DOPA-free (HAGM and GelMA) cryogels (**Fig 3**). Specifically, key physical properties such as mechanical compression (**Fig 3A**), extensibility (**Fig 3B**), swelling (**Fig 3C**), and the degree of pore connectivity (**Fig 3D**) were measured. Optimized parameters previously defined were utilized for the comparison: 4% polymer concentration with GSH (20 mM) in the prepolymer solution using 2 mM AD or APD. As such, compressive moduli of HAGM, HD, and HPD resulted in 1.5 ± 0.8 kPa, 1.3 ± 0.8 kPa, and 1.1 ± 0.8 kPa, respectively.

Similarly, GelMA, GD, and GPD displayed compressive moduli of 5.6 ± 1.9 kPa, 6.0 ± 1.5 kPa, and 6.4 ± 1.2 kPa, respectively (**Fig 3A**). Regardless of the incorporation of polymerizable DOPA (AD or APD) prior to cryogelation, the compressive moduli were unaltered for both HAGM and GelMA-based cryogels. However, the Young's moduli increased by one order of magnitude when AD or APD were added (**Fig 3B**). Notably, HAGM, HD, and HPD had Young's moduli of 2.3 ± 0.8 kPa, 23.6 ± 1.0 kPa, and 41.6 ± 0.8 kPa, respectively. Similarly, GelMA, GD, and GPD exhibited Young's moduli of 8.3 ± 1.9 kPa, 32.4 ± 2.3 kPa, and 65.6 ± 1.2 kPa, respectively. This highlights the advantages of adding AD or APD in the prepolymer formulation to improve the tensile strength and elasticity of HAGM and GelMA-based cryogels. Our set of data agrees with the literature as DOPA-containing biomaterials are known to display super stretchability and self-healing properties [50], most likely due to reversible noncovalent bonds formed between the catechol groups of pendant DOPA moieties along the polymer network, including π - π stacking and hydrogen bonds.

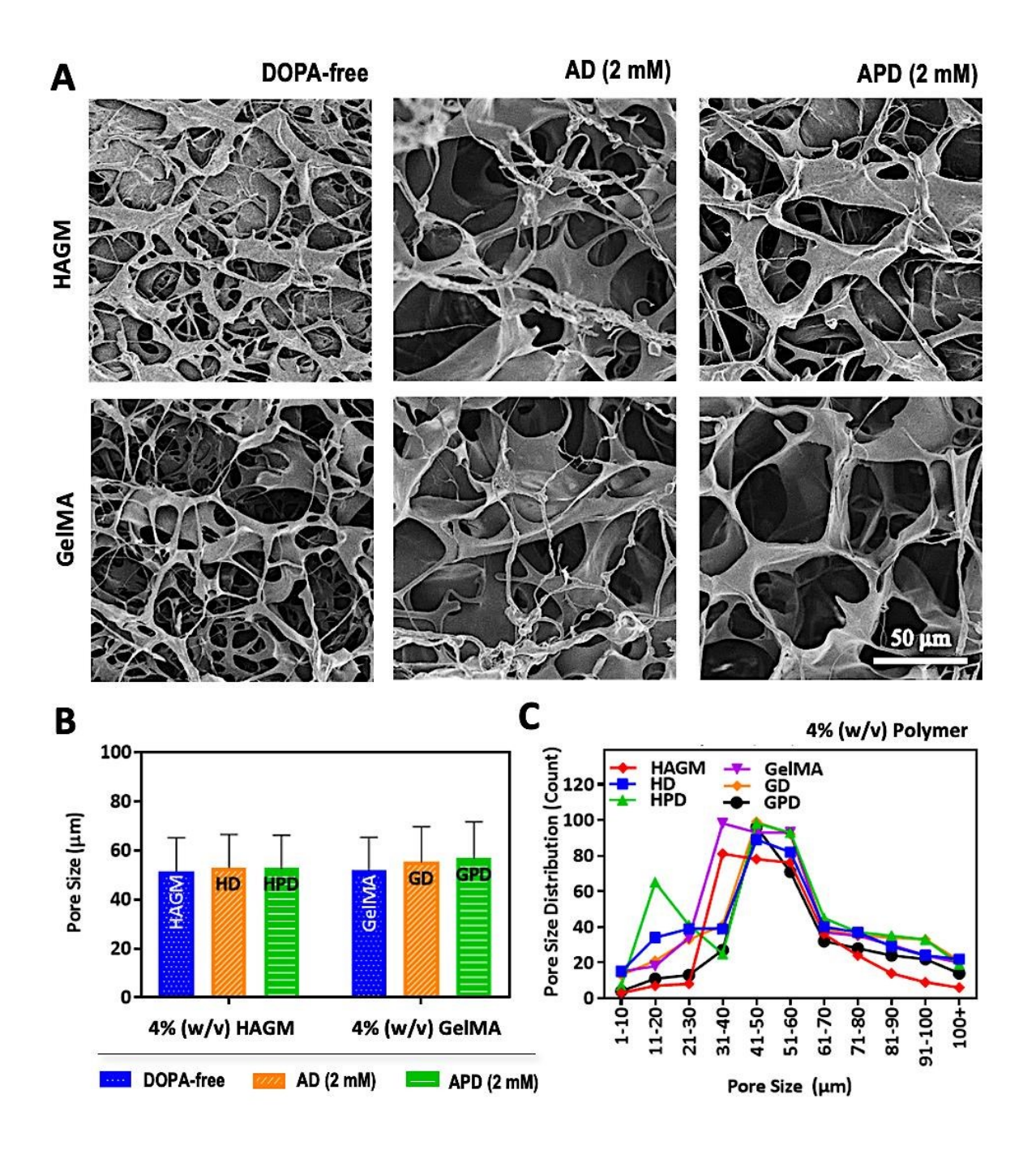


Figure 4. Microstructural features of bioadhesive HAGM and GelMA-based cryogels. Representative SEM images (A), pore size (B), and pore size distribution (C) of HAGM and GelMA-based DOPA-containing (i.e., AD or APD) cryogels. HAGM: DOPA-free HAGM, GelMA: DOPA-free GelMA, HD: AD-containing HAGM, HPD (APD-containing HAGM), GD (AD-containing GelMA), GPD (APD-containing GelMA). Values represent the mean \pm SD (n = 5).

Next, we evaluated the swelling behavior at equilibrium since bioadhesive cryogels can retain a significant fraction of water within their structures. Overall, HAGM and GelMA-based cryogels exhibited similar swelling ratios regardless of AD or APD incorporation. Specifically, HAGM, HD, and HPD cryogels resulted in $Q_M = 42.5 \pm 5.1$, 29.9 ± 3.4 , and 40.9 ± 3.9 , respectively. Similarly, GelMA, GD, and GPD cryogels displayed $Q_M = 45.3 \pm 8.8$, 34.5 ± 8.5 , and 47.6 ± 8.4 , respectively (**Fig 3C**). The consistent swelling rates may suggest the fine control over pore size formation during cryogelation and similar hydrophilicity, regardless of the biopolymer used. Additionally, the degree of pore connectivity, another important physical property, was evaluated for each cryogels fabricated in this study and is shown in **Fig 3D**. HAGM and GelMA cryogels demonstrated high pore connectivity of $77.9 \pm 0.1\%$ and $75.4 \pm 0.1\%$, respectively. Similarly, DOPA-containing HAGM and GelMA (HD, HPD, GD, and GPD) cryogels exhibited similar degrees of pore connectivity ranging from $70.8 \pm 0.05\%$ to $78.9 \pm 0.08\%$, highlighting the integrity of cryogels (**Fig 3D**).

The ability of spherical and cuboidal bioadhesive cryogels (**Fig S5**) to be injected through conventional hypodermic needles and regain their original shapes once delivered was also evaluated. Due to their inherent properties, DOPA-containing cryogels can be reversibly collapsed (up to 90% of their volume), owing to their highly macroporous structure and mechanical robustness, and be pushed through the needle with no visible fracture or damage (**Fig 3E**). After injection, the deformed bioadhesive cryogels rapidly returned to their original, undeformed configurations (**Videos S2** and **S3**), reabsorbing surrounding water into the gels. This is a critical property for minimally invasive procedures.

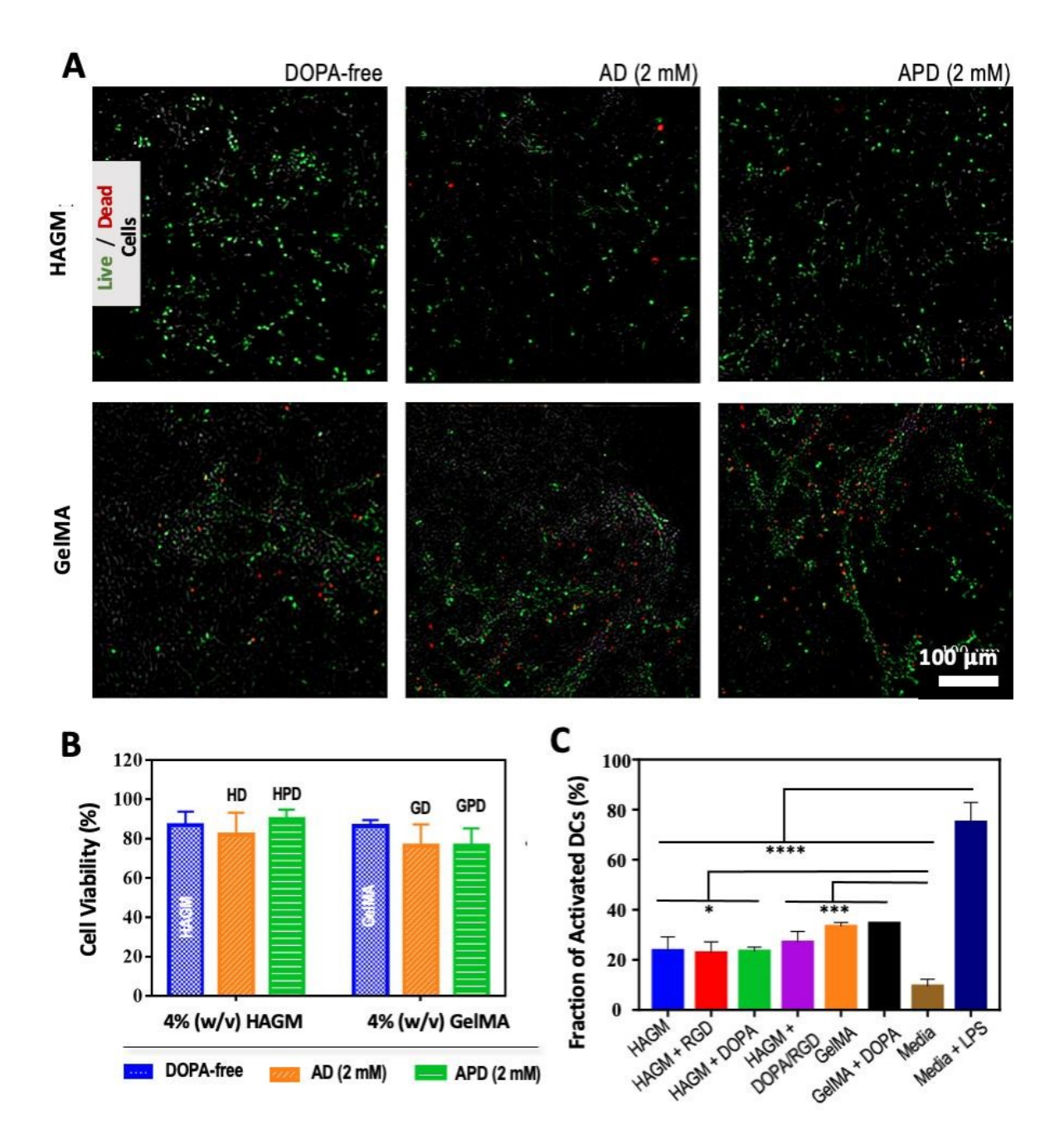


Figure 5. Evaluating the cytocompatibility of bioadhesive HAGM and GelMA-based cryogels. (A) Confocal images showing mouse embryonic fibroblast NIH/3T3 cells cultured for 24 h in DOPA-free and DOPA-containing (i.e., AD and APD) HAGM and GelMA-based cryogels. (B) Green and red colors depict viable and dead cells, respectively. Quantification of cell viability of NIH 3T3 cells. (C) Fractions of activated CD11c⁺ CD86⁺ MHCII⁺ BMDCs after 24 h of incubation in the different conditions: HAGM (DOPA-free) cryogels, HAGM + RGD (DOPA-free, APR-containing) cryogels, HAGM + DOPA (HD:

APD-containing HAGM) cryogels, HAGM + DOPA/RGD (HD + APR: RGD-containing, APD-containing HAGM) cryogels, GelMA (DOPA-free) cryogels, GelMA + DOPA (GDP: APD-containing GelMA) cryogels, cell culture media (RPMI 1640, negative control), and cell culture media + lipopolysaccharide (RPMI 1640 + LPS, negative control). Values represent the mean \pm SD and data were analyzed using oneway ANOVA (n = 5). *p < 0.05, ***p < 0.001, and ****p < 0.0001.

Cryogels are 3D hydrogels consisting of a network of interconnected macropores. As shown in **Figs 4A and S6**, all cryogels (HAGM, HD, HPD, GelMA, GD, and GPD) displayed an interconnected macroporous network with thick polymer walls. SEM imaging demonstrated average pore sizes in the range of ~50 μm (**Fig 4B**). Although not statistically significant, the incorporation of AD and APD in cryogels led to a slight increase in pore size diameter. Comparatively, the overall pore size distribution revealed pore sizes ranging from 1 to over 100 μm, with most pores in the range of 30 to 70 μm (**Fig 4C**). It should be noted that confocal images depicted slightly smaller pore sizes, most likely due to partial dehydration of the cryogel samples throughout the imaging process.

3.4. *In vitro* **cytocompatibility of bioadhesive cryogels.** Our cryogels with optimized formulations for high bioadhesion were tested for their cytocompatibility with mouse embryonic fibroblast NIH/3T3 cells. Specifically, 4% (w/v) RGD-bearing HAGM and GelMA-based DOPA-containing cryogels (i.e., 2mM AD or APD) prepared with GSH were evaluated for cytotoxicity.

As shown in **Fig 5A**, the bioadhesive cryogels provided an appropriate microenvironment for cell attachment and survival leading to ~80% viability after 1 day of incubation (**Fig 5B**). The formation of a monolayer of cells on the surface of all cryogels, especially on GelMA-based cryogels, suggests uniform seeding and retention of cells through the open-pore structure of the

constructs. Furthermore, cells exhibited an elongated and stretched morphology as depicted in the confocal images.

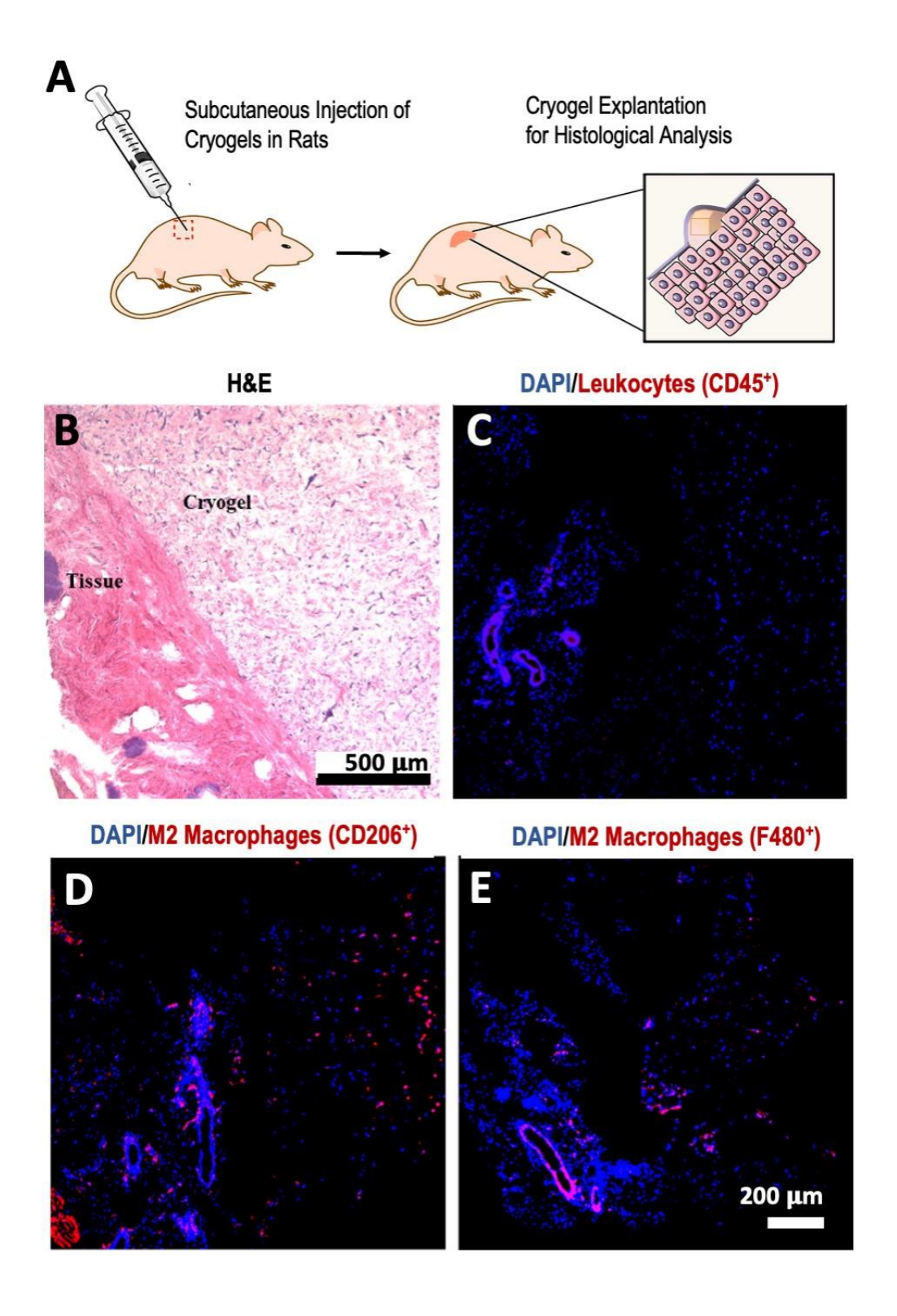


Figure 6. Evaluating the biocompatibility of bioadhesive HAGM-based cryogels. (**A**) Illustration depicting the subcutaneous injection and explantation of bioadhesive HAGM-based DOPA-containing (i.e., APD) cryogels in the dorsal flanks of Wistar rats. (**B**) Representative H&E staining of cryogel sections explanted 21 days following injections. Fluorescent immunohistochemical analysis of stained cryogels to assess the infiltration of CD45⁺ leukocytes (**C**) and CD206⁺ (**D**) and F4/80⁺ (**E**) macrophages.

Another simple method for evaluating the cytocompatibility of biomaterials is to perform *in vitro* assay with immune cells such as DCs. DCs play a critical role in the regulation of the adaptive immunity, as they are known to secrete various proinflammatory cytokines upon maturation [51]. As an alternative *in vitro* technique for biocompatibility studies, cryogels were assessed for their immunogenicity with BMDCs. The fraction of activated CD11c⁺CD86⁺MHCII⁺BMDCs was detected by immunostaining in conjunction with flow cytometry after 1 day of culture with the cryogels. Overall, all cryogels tested induced low-expression profiles of CD11c, CD86, and MHCII receptors when compared to LPS, our positive control (**Fig 5C**). Unlike HA-based cryogels, GelMA-based cryogels induced a slightly higher stimulation of DCs, most likely due to partial degradation and release of small fragments [17]. These results collectively demonstrate the capacity of bioadhesive cryogels to serve as a cell-friendly and biomimetic scaffold.

3.5 *In vivo* injectability and immunohistological analysis of bioadhesive cryogels. As an essential component of implant performance, we examined the host immune response to HAGM-based DOPA-containing cryogels, a selected bioadhesive cryogel candidate with high performance and *in vitro* biocompatibility. Specifically, we characterized the *in vivo* performance of HPD cryogels, including their integration with native tissues, eventual biodegradation, and potential inflammation following their subcutaneous implantation in an animal model. As shown in **Fig 6A**,

sterile cuboidal cryogels (dimensions: 4 x 4 x 1 mm³) were subcutaneously injected using a 16-gauge needle in the backs of Wistar rats. At day 21 post-implantation, cryogels which appeared to remain partially intact were explanted with adjacent tissues for analysis. H&E staining showed a mild inflammatory reaction. As depicted in **Fig 6B**, the cryogel scaffold exhibit a highly porous network surrounded by a layer of fibrin and few cells. Furthermore, an immunocytochemistry analysis further confirmed a negligible leukocyte infiltration as demonstrated by a relatively low number of CD45⁺ cells (**Fig 6C**). In contrast, although minimal, we observed some infiltration of CD206⁺ and F4/80⁺ macrophages within the cryogel constructs (**Figs 6D** and **6E**). This slight inflammatory response is most likely due to the subcutaneous administration [52]. As with any injection, this mode of administration can be associated with local pain and irritation from the needle puncture. Overall, in agreement with our *in vitro* assay with primary immune cells (**Fig 5C**), these preclinical data indicate that the bioadhesive cryogels induce a minimal immune reaction at the implantation site, indicating biocompatibility.

Discussion

A minimally invasive approach can be implemented to deliver bioadhesive and preformed shapememory macroporous cryogels via needle-syringe injection into the body. These adhesive cryogels could be readily injected into the subcutaneous layer of the skin to potentially fill *in vivo* tissue defects and cavities or used as injectable patches on internal or external organs, while their adhesiveness could hold biological tissues in place. Our *in vivo* study was primarily conducted to assess the biocompatibility rather than the bioadhesive properties of DOPA-containing cryogels. While we observed good integration of DOPA-containing cryogels with the surrounding tissues, further preclinical studies would be required to test their *in vivo* bioadhesive properties to a dynamic organ such as the heart which undergoes large and repetitive volumetric deformations. For instance, to treat myocardial infarction, T. Wu *et al.* have engineered an injectable and bioadhesive gelatin hydrogel-based patch for heart repair, resulting in improved cardiac function [53].

Cryogels exhibit an interconnected macroporous network, which is advantageous for a scaffold system with respect to their ability to promote cellular adhesion and infiltration, increase vascularization, facilitate diffusion of nutrients and oxygen, and ultimately enhance tissue regeneration. Furthermore, these biomaterials also offer the potential for carrying payloads (i.e., cells, drugs, nanoparticles) after being manufactured [18] and would be of interest in future studies in conjunction with their strong adhesive properties. The most important requirement for cryogels for minimally invasive delivery is their ability to be compressed up to 90% of their original volume. Due to their shape memory properties, cryogels can reliably and quickly recover their original size and shape once placed in the body via the uptake of exudate and injection of saline. Furthermore, the ability of these materials to reassume specific, predefined shapes after injection is likely to be useful in applications such as tissue patches (i.e., cardiac patches), ulcers, cartilage replacement, plastic surgery, fat replacement, oral surgeries, and voids left behind from tumor and tissue removals. Specifically, this is of interest where one desires a specific volume defect site to be filled with a biomaterial that can pull the adjacent tissue walls together. Alternatively, multiple smaller and packable adhesive cryogels can be used for large defects while allowing diffusional transport and vascularization [54, 55]. Because of the ability to tune the adhesive properties by controlling the amount of AD or APD used as comonomers during cryopolymerization, this can be achieved with fine control. Furthermore, the elastic properties of cryogels enhance their attachment to tissues while the adhesive strength may support tissue contraction and facilitate tissue regeneration – similar to the function of sutures or staples. Additionally, the use of biodegradable polymers such as HA and gelatin, no secondary surgical procedure is needed to remove the cryogels [23]. Although previous work has shown that HAGM and GelMA-based cryogels are susceptible to biodegradation [23, 56], more research is required to better understand the degradation profiles of these bioadhesive cryogels and how they correlate with tissue repair in an *in vivo* context.

Cryogels display soft tissue-like mechanical properties due to their inherent porous structure in combination with a highly crosslinked polymer network due to methacrylated biopolymers, nearly complete reactivity of methacryoyl groups during cryogelation, sterically entangled polymer chains, and the extent of phase separation during cryopolymerization. Unlike their mesoporous hydrogel counterpart, the unique macrostructure of cryogels allows them to be highly compressible, resulting in injectable scaffolds. As previously stated, free water contained within the pores of the cryogel can be expunged upon compression and then reabsorbed upon reversal of compression. This compression and release can be conducted without any physical damage to the walls of cryogels. However, it was noticed that beyond 90% compression, each incremental further compressive force applied creates an inverse vacuum or suction effect which forces cryogel walls to "stick" together. Thereby taking a longer time to reuptake liquid once submerged. Furthermore, once all cryogel walls are fully collapsed, further compressive strain results in wall failure.

The cryogels can be created in any desired shape and size. These locked-in features, resulting in shape memory, are retained through the process of syringe injection without being compromised [18, 41, 57, 58]. Furthermore, the bioadhesive cryogels were fabricated with HA and gelatin but can potentially be fabricated with various synthetic and naturally derived polymers, as highlighted in Table S1. One could further tune the performance of cryogels by altering their composition, formulation, and chemistry. The ability of these cryogels to be syringe delivered at a specific location without the need for an invasive surgery may decrease scarring, lessen the risk of infections, and reduce recovery times compared with traditional procedures, which typically require a secondary surgery or the use of secondary sealants, staples, or sutures [26, 28, 30]. As depicted in Table S1 the cryogels reported here possess higher adhesion strengths than previously published DOPA-containing hydrogels and cryogels. This highlights a significant decrease in adhesion strength just by incorporating DOPA without functionalization. As previously reported, the simple addition of DOPA causes autooxidation and formation of PDA, resulting in the depletion of potential binding sites (i.e., catechol residues) and reduction of tissue adhesion [26]. This is in stark contrast to the readily accepted notion that adding DOPA would readily increase adhesion.

These bioadhesive cryogels could act as delivery vehicles for therapeutics and cells over a sustained period [18, 41]. By providing a protein drug depot at the injection site, cryogels can potentially achieve high local protein concentrations without systemic exposure. Biomolecules can be physically entrapped during the cryopolymerization and later released in sustained fashion [21, 23, 44].

The chemical modification of DOPA and use of a PEG spacer are techniques that can be scaled up and applied to other non-catechol-based wet adhesives that adhere via electrostatic interactions, hydrogen bonding, dynamic covalent bonding, as well topological entanglement. Herein, we described a method in which amine-bearing DOPA was functionalized, thereby limiting its reactivity (autoxidative power) in aqueous solutions. This enabled DOPA to be copolymerized with functionalized biopolymers (HAGM and GelMA) to enhance adhesion in wet environments. However, it was observed that the adhesion strength decreases at high APD concentration. This could be attributable to a "brush conformation" resulting from higher PEGlinker concentrations, which may lead to steric hinderances from an overcrowded network [59]. The PEG-linkers, originally used to reduce steric hindrance, due to "short" DOPA molecules, could themselves be an impediment at high density, potentially compromising the bioadhesion strength [56]. However, more research is required to be better understand the surface topography of DOPA-containing cryogels and confirm whether the brush conformation effect induces weaker bioadhesion. Furthermore, we believe that adhesion was improved due to retaining catechol residues intact in an oxidation-free environment. These binding sites are typically consumed during the unwanted oxidation-mediated polymerization of DOPA into PDA [60-63]. It has previously been reported that decreasing or preventing DOPA oxidation resulted in greater adhesion of DOPA-containing hydrogels [64]. Therefore, we incorporated GSH into our formulation to prevent or reduce the oxidation of DOPA [34]. Preventing DOPA oxidation resulting in the non-browning of the resulting cryogels, increased viability of cells known to be sensitive to oxidized DOPA. Overall, these strategies led to the design of DOPA-containing cryogels with very strong adhesion properties to several organs and tissues, lifting up to \sim 60 times their own weights.

DOPA-containing cryogels offer various unique advantages over existing biomaterials with similar or higher bioadhesive strength. DOPA-containing cryogels achieved a lap sheer strength of 15.5 ± 0.4 kPa, surpassing commercially available bioadhesives such as Evicel® (13.2 ± 2.3 kPa) and CoSeal® (9.6 ± 8.7 kPa). While a number of mussel-inspired catechol-based hydrogels such as DOPA-conjugated tendon extracellular matrix [65], DOPA-conjugated poly(γ-glutamic acid) [66], and a glucose-based 3-O-methyl-DOPA-containing bioadhesive have been reported to exhibit higher lap sheer strengths, DOPA-containing cryogels offer several advantages such as syringe-injectability [67], a preformed gel system, shape-memory features, a macroporous and interconnected network, and/or unoxidized (i.e., browning-free) environment.

A challenge in the design of bioadhesive cryogels is specificity as non-specific tissue adhesions could potentially lead to complications in a clinical setting. DOPA-containing cryogels are designed to adhere to any biological tissues or organs. However, it would be advantageous when required to have cryogels or any biomaterials for that matter that can controllably and adhere to a target tissue *in vivo* without simultaneously adhering to surrounding tissues. Engineering cryogels with gradient adhesion or defined adhesive areas could potentially achieve such adhesion to a target tissue or organs.

When transitioning from preclinical research to clinical practice, where larger constructs are frequently needed for human use, the size of injectable cryogels could be a challenge. To overcome this limitation, several strategies are currently being investigated, including examining

various crosslinking methods and cryogel geometries as well as optimizing the macrostructural characteristics of cryogels (e.g., pore size, pore connectivity, pore orientation, toughness, and flexibility). Future cryogel development should increase their biological utility and improve clinical translation by creating cryogels with well-defined macrostructural features, smart cryogels sensitive to environmental stimuli, and more compressible or self-healing cryogels.

Conclusion

In this study, we developed injectable and highly bioadhesive mussel-inspired cryogels to serve as biomimetic scaffolds for tissue engineering and regenerative medicine. These cryogels were prepared from HA and gelatin and were functionalized with DOPA to impart bioadhesive properties. These minimally invasive catechol-containing cryogels demonstrated high adhesion to wet surfaces and excellent elasticity and mechanical properties to support the stretching or bending of tissues. Additionally, we described a strategy to prevent the oxidation of DOPA, mitigating browning while increasing the bioadhesive strength of catechol residues as shown with the striking adhesion tests on large animal tissues and organs such as the heart, small intestine, lung, kidney, and skin. *In vitro* and *in vivo* studies confirmed high cytocompatibility as well as good tissue integration and a minimal host inflammatory response when cryogels were subcutaneously injected in rats. Overall, bioadhesive and minimally invasive cryogels could potentially be used as scaffolds for wound closure and sealing while restoring, maintaining, or improving impaired tissues and organs.

CRediT authorship contribution statement

Devyesh Rana: Conceptualization, Methodology, Validation, Investigation, Data curation, Visualization, Writing – original draft & editing. Bahram Saleh: Methodology. Thibault Colombani: Methodology, Validation. Halimatu Mohammad: Writing – review & editing. Nasim Annabi: Conceptualization, Supervision, Funding acquisition. Sidi A. Bencherif: Conceptualization, Supervision, Project administration, Funding acquisition, Writing – review & editing.

Declaration of interests

The authors declare that they have no known competing financial interests or personal relationships that could have appeared to influence the work reported in this paper.

Acknowledgment

This project has received funding from the National Institutes of Health (1R01EB027705) and the National Science Foundation (DMR 1847843).

Data availability

The data that support the findings of this study are available from the corresponding author upon reasonable request.

References

- 1. Rahimnejad, M., Zhong, W., Mussel-inspired hydrogel tissue adhesives for wound closure, RSC Advances. (2017) 7 (75), 47380
- 2. Wheat, J. C., Wolf, J. S., Jr., Advances in bioadhesives, tissue sealants, and hemostatic Agents, Urologic Clinics. (2009) **36** (2), 265
- 3. Mehdizadeh, M., Weng, H., Gyawali, D., Tang, L., Yang, J., Injectable citrate-based mussel-inspired tissue bioadhesives with high wet strength for sutureless wound closure, Biomaterials. (2012) **33** (32), 7972
- 4. Spotnitz, W. D., Fibrin Sealant: Past, present, and future: A Brief review, World Journal of Surgery. (2010) **34** (4), 632
- 5. Radosevich, M., Goubran, H. A., Burnouf, T., Fibrin Sealant: Scientific Rationale, Production Methods, Properties, and Current Clinical Use, Vox Sanguinis. (1997) 72 (3), 133
- 6. Joch, C., The safety of fibrin sealants, Cardiovascular Surgery. (2003) 11, 23
- 7. Traver, M. A., Assimos, D. G., New generation tissue sealants and hemostatic agents: Innovative urologic applications, Reviews in Urology. (2006) 8 (3), 104
- 8. Lee, K. Y., Mooney, D. J., Hydrogels for tissue engineering, Chemical Reviews. (2001) 101 (7), 1869
- 9. Bencherif, S. A., Srinivasan, A., Horkay, F., Hollinger, J. O., Matyjaszewski, K., Washburn, N. R., Influence of the degree of methacrylation on hyaluronic acid hydrogels properties, Biomaterials. (2008) **29** (12), 1739
- 10. Prata, J. E., Barth, T. A., Bencherif, S. A., Washburn, N. R., Complex fluids based on methacrylated hyaluronic acid, Biomacromolecules. (2010) 11 (3), 769
- 11. Gsib, O., Eggermont, L. J., Egles, C., Bencherif, S. A., Engineering a macroporous fibrin-based sequential interpenetrating polymer network for dermal tissue engineering, Biomaterials Science. (2020) 8 (24), 7106
- 12. Gsib, O., Duval, J. L., Goczkowski, M., Deneufchatel, M., Fichet, O., Larreta-Garde, V., Bencherif, S. A., Egles, C., Evaluation of fibrin-based interpenetrating polymer networks as potential biomaterials for tissue engineering, Nanomaterials (Basel). (2017) 7 (12)
- 13. Gsib, O., Egles, C., Bencherif, S., Fibrin: An Underrated biopolymer for skin tissue engineering, Journal of Molecular Biology and Biotechnology. (2017) 1, 1
- 14. Yoon, J. A., Bencherif, S. A., Aksak, B., Kim, E. K., Kowalewski, T., Oh, J. K., Matyjaszewski, K., Thermoresponsive hydrogel scaffolds with tailored hydrophilic pores, Chemistry: An Asian Journal. (2011) 6 (1), 128
- 15. Rogers, Z. J., Zeevi, M. P., Koppes, R., Bencherif, S. A., Electroconductive Hydrogels for Tissue Engineering: Current Status and Future Perspectives, Bioelectricity. (2020) **2** (3), 279
- 16. Eggermont, L. J., Rogers, Z. J., Colombani, T., Memic, A., Bencherif, S. A., Injectable cryogels for biomedical applications, Trends in biotechnology. (2020) **38** (4), 418
- 17. Rezaeeyazdi, M., Colombani, T., Memic, A., Bencherif, S. A., Injectable hyaluronic acid-co-gelatin cryogels for tissue engineering applications, Materials. (2018) 11 (8), 1374
- 18. Bencherif, S. A., Sands, R. W., Bhatta, D., Arany, P., Verbeke, C. S., Edwards, D. A., Mooney, D. J., Injectable preformed scaffolds with shape-memory properties, PNAS. (2012) **109** (48), 19590

- Colombani, T., Eggermont, L. J., Hatfield, S. M., Rogers, Z. J., Rezaeeyazdi, M., Memic, A., Sitkovsky, M. V., Bencherif, S. A., Oxygen-generating cryogels restore t cell mediated cytotoxicity in hypoxic tumors, Advanced Functional Materials. (2021) 31 (37), 2102234
- Colombani, T., Eggermont, L. J., Rogers, Z. J., McKay, L. G. A., Avena, L. E., Johnson, R. I., Storm, N., Griffiths, A., Bencherif, S. A., Biomaterials and oxygen join forces to shape the immune response and boost COVID-19 vaccines, Advanced Science. (2021) 8 (18), 2100316
- 21. Colombani, T., Rogers, Z. J., Eggermont, L. J., Bencherif, S. A., Harnessing biomaterials for therapeutic strategies against COVID-19, Emergent materials. (2021) 4 (1), 9
- 22. Boulais, L., Jellali, R., Pereira, U., Leclerc, E., Bencherif, S. A., Legallais, C., Cryogel-integrated biochip for liver tissue engineering, ACS Applied Bio Materials. (2021) 4 (7), 5617
- 23. Joshi Navare, K., Colombani, T., Rezaeeyazdi, M., Bassous, N., Rana, D., Webster, T., Memic, A., Bencherif, S. A., Needle-injectable microcomposite cryogel scaffolds with antimicrobial properties, Scientific Reports. (2020) **10** (1), 18370
- 24. He, T., Li, B., Colombani, T., Joshi-Navare, K., Mehta, S., Kisiday, J., Bencherif, S. A., Bajpayee, A. G., Hyaluronic acid-based shape-memory cryogel scaffolds for focal cartilage defect repair, Tissue Engineering Part A. (2021) 27 (11-12), 748
- 25. Memic, A., Rezaeeyazdi, M., Villard, P., Rogers, Z. J., Abudula, T., Colombani, T., Bencherif, S. A., Effect of Polymer Concentration on autoclaved cryogel properties, macromolecular materials and engineering. (2020) **305** (5), 1900824
- Memic, A., Colombani, T., Eggermont, L. J., Rezaeeyazdi, M., Steingold, J., Rogers, Z. J., Navare, K. J., Mohammed, H. S., Bencherif, S. A., Latest advances in cryogel technology for biomedical applications, advanced therapeutics. (2019) 2 (4), 1800114
- 27. Kennedy, S., Bencherif, S., Norton, D., Weinstock, L., Mehta, M., Mooney, D., Rapid and extensive collapse from electrically responsive macroporous hydrogels, Advanced Healthcare Materials. (2014) **3** (4), 500
- 28. Rogers, Z. J., Bencherif, S. A., Cryogelation and cryogels, Gels (Basel, Switzerland). (2019) 5 (4)
- 29. Joshi Navare, K., Eggermont, L. J., Rogers, Z. J., Mohammed, H. S., Colombani, T., Bencherif, S. A., Antimicrobial hydrogels: Key considerations and engineering strategies for biomedical applications. In *Racing for the Surface: Pathogenesis of Implant Infection and Advanced Antimicrobial Strategies*, Li, B., et al., (eds.) Springer International Publishing, Cham, (2020), pp 511
- 30. Eggermont, L. J., Rogers, Z. J., Colombani, T., Memic, A., Bencherif, S. A., Injectable cryogels for biomedical applications, Trends in biotechnology. (2020) **38** (4), 418
- 31. Konovalova, M. V., Markov, P. A., Popova, G. Y., Nikitina, I. R., Shumikhin, K. V., Kurek, D. V., Varlamov, V. P., Popov, S. V., Prevention of postoperative adhesions by biodegradable cryogels from pectin and chitosan polysaccharides, Journal of Bioactive and Compatible Polymers. (2017) 32 (5), 487
- 32. Peppas, N. A., Sahlin, J. J., Hydrogels as mucoadhesive and bioadhesive materials: a review, Biomaterials. (1996) 17 (16), 1553
- 33. Cui, C., Liu, W., Recent advances in wet adhesives: Adhesion mechanism, design principle and applications, Progress in Polymer Science. (2021) 116, 101388
- 34. Rana, D., Colombani, T., Mohammed, H. S., Eggermont, L. J., Johnson, S., Annabi, N., Bencherif, S. A., Strategies to prevent dopamine oxidation and related cytotoxicity using various antioxidants and nitrogenation, Emergent Materials. (2019) 2 (2), 209
- 35. Rezaeeyazdi, M., Colombani, T., Eggermont, L. J., Bencherif, S. A., Engineering hyaluronic acid-based cryogels for CD44-mediated breast tumor reconstruction, Materials Today Bio. (2022) **13**, 100207

- 36. Villard, P., Rezaeeyazdi, M., Colombani, T., Joshi-Navare, K., Rana, D., Memic, A., Bencherif, S. A., Autoclavable and injectable cryogels for biomedical applications, Advanced Healthcare Materials. (2019) 8 (17), 1900679
- 37. Annabi, N., Rana, D., Shirzaei Sani, E., Portillo-Lara, R., Gifford, J. L., Fares, M. M., Mithieux, S. M., Weiss, A. S., Engineering a sprayable and elastic hydrogel adhesive with antimicrobial properties for wound healing, Biomaterials. (2017) **139**, 229
- 38. Kim, J., Bencherif, S. A., Li, W. A., Mooney, D. J., Cell-Friendly Inverse Opal-Like Hydrogels for a spatially separated co-culture system, Macromolecular Rapid Communications. (2014) **35** (18), 1578
- 39. F2458–05(2015), A., Standard test method for wound closure strength of tissue adhesives and sealants, ASTM International. (2015) **13** (01)
- 40. F2393-04(2015), A., Standard test method for burst strength of surgical sealants, ASTM International. (2015) **12** (01)
- 41. Bencherif, S. A., Warren Sands, R., Ali, O. A., Li, W. A., Lewin, S. A., Braschler, T. M., Shih, T.-Y., Verbeke, C. S., Bhatta, D., Dranoff, G., Mooney, D. J., Injectable cryogel-based whole-cell cancer vaccines, Nature Communications. (2015) 6 (1), 7556
- 42. Annabi, N., Shin, S. R., Tamayol, A., Miscuglio, M., Bakooshli, M. A., Assmann, A., Mostafalu, P., Sun, J.-Y., Mithieux, S., Cheung, L., Tang, X., Weiss, A. S., Khademhosseini, A., Highly Elastic and conductive human-based protein hybrid hydrogels, Advanced Materials. (2016) **28** (1), 40
- 43. Yue, K., Trujillo-de Santiago, G., Alvarez, M. M., Tamayol, A., Annabi, N., Khademhosseini, A., Synthesis, properties, and biomedical applications of gelatin methacryloyl (GelMA) hydrogels, Biomaterials. (2015) 73, 254
- 44. Lee, H., Scherer, N. F., Messersmith, P. B., Single-molecule mechanics of mussel adhesion, PNAS. (2006) **103** (35), 12999
- 45. Shin, E. D., Estall, J. L., Izzo, A., Drucker, D. J., Brubaker, P. L., Mucosal adaptation to enteral nutrients is dependent on the physiologic actions of glucagon-like peptide-2 in mice, Gastroenterology. (2005) **128** (5), 1340
- 46. Marini, J. J., Recruitment by sustained inflation: time for a change, Intensive Care Medicine. (2011) **37** (10), 1572
- 47. Hill, A., Estridge, T. D., Maroney, M., Monnet, E., Egbert, B., Cruise, G., Coker, G. T., Treatment of suture line bleeding with a novel synthetic surgical sealant in a canine iliac PTFE graft model, Journal of biomedical materials research. (2001) **58** (3), 308
- 48. Wallace, D. G., Cruise, G. M., Rhee, W. M., Schroeder, J. A., Prior, J. J., Ju, J., Maroney, M., Duronio, J., Ngo, M. H., Estridge, T., Coker, G. C., A tissue sealant based on reactive multifunctional polyethylene glycol, Journal of biomedical materials research. (2001) **58** (5), 545
- 49. Annabi, N., Zhang, Y.-N., Assmann, A., Sani, E. S., Cheng, G., Lassaletta, A. D., Vegh, A., Dehghani, B., Ruiz-Esparza, G. U., Wang, X., Gangadharan, S., Weiss, A. S., Khademhosseini, A., Engineering a highly elastic human protein based sealant for surgical applications, Science Translational Medicine. (2017) 9 (410)
- 50. Han, L., Yan, L., Wang, K., Fang, L., Zhang, H., Tang, Y., Ding, Y., Weng, L.-T., Xu, J., Weng, J., Liu, Y., Ren, F., Lu, X., Tough, self-healable and tissue-adhesive hydrogel with tunable multifunctionality, NPG Asia Materials. (2017) 9 (4), 372
- 51. Groell, F., Kalia, Y. N., Jordan, O., Borchard, G., Hydrogels in three-dimensional dendritic cell (MUTZ-3) culture as a scaffold to mimic human immuno competent subcutaneous tissue, International Journal of Pharmaceutics. (2018) **544** (1), 297

- 52. St. Clair-Jones, A., Prignano, F., Goncalves, J., Paul, M., Sewerin, P., Understanding and minimising injection-site pain following subcutaneous administration of biologics: A narrative review, Rheumatology and therapy. (2020) 7 (4), 741
- 53. Wu, T., Cui, C., Huang, Y., Liu, Y., Fan, C., Han, X., Yang, Y., Xu, Z., Liu, B., Fan, G., Liu, W., Coadministration of an adhesive conductive hydrogel patch and an injectable hydrogel to treat myocardial infarction, ACS Applied Materials & Interfaces. (2020) 12 (2), 2039
- 54. Leor, J., Amsalem, Y., Cohen, S., Cells, scaffolds, and molecules for myocardial tissue engineering, Pharmacology & Therapeutics. (2005) **105** (2), 151
- 55. Halberstadt, C., Austin, C., Rowley, J., Culberson, C., Loebsack, A., Wyatt, S., Coleman, S., Blacksten, L., Burg, K., Mooney, D., Jr., W. H., A hydrogel material for plastic and reconstructive applications injected into the subcutaneous space of a sheep, Tissue Engineering. (2002) 8 (2), 309
- 56. Koshy, S. T., Ferrante, T. C., Lewin, S. A., Mooney, D. J., Injectable, porous, and cell-responsive gelatin cryogels, Biomaterials. (2014) **35** (8), 2477
- 57. Yuan, Z., Yuan, X., Zhao, Y., Cai, Q., Wang, Y., Luo, R., Yu, S., Wang, Y., Han, J., Ge, L., Huang, J., Xiong, C., Injectable GelMA cryogel microspheres for modularized cell delivery and potential vascularized bone regeneration, Small. (2021) 17 (11), 2006596
- 58. Yuan, X., Yuan, Z., Wang, Y., Wan, Z., Wang, X., Yu, S., Han, J., Huang, J., Xiong, C., Ge, L., Cai, Q., Zhao, Y., Vascularized pulp regeneration via injecting simvastatin functionalized GelMA cryogel microspheres loaded with stem cells from human exfoliated deciduous teeth, Materials Today Bio. (2022) 13, 100209
- 59. Li, M., Jiang, S., Simon, J., Paßlick, D., Frey, M.-L., Wagner, M., Mailänder, V., Crespy, D., Landfester, K., Brush conformation of polyethylene glycol determines the stealth effect of nanocarriers in the low protein adsorption regime, Nano Letters. (2021) **21** (4), 1591
- 60. Munoz, P., Huenchuguala, S., Paris, I., Segura-Aguilar, J., Dopamine oxidation and autophagy, Parkinsons Disease. (2012) **2012**, 13
- 61. Segura-Aguilar, J., Paris, I., Mechanisms of dopamine oxidation and parkinson's disease. In *Handbook of Neurotoxicity*, Kostrzewa, R. M., (ed.) Springer New York, New York, NY, (2014), pp 865
- 62. Ding, Y. H., Floren, M., Tan, W., Mussel-inspired polydopamine for bio-surface functionalization, Biosurface and Biotribology. (2016) **2** (4), 121
- 63. Liebscher, J., Mrówczyński, R., Scheidt, H. A., Filip, C., Hădade, N. D., Turcu, R., Bende, A., Beck, S., Structure of polydopamine: A never-ending story?, Langmuir. (2013) **29** (33), 10539
- 64. Cencer, M., Liu, Y., Winter, A., Murley, M., Meng, H., Lee, B. P., Effect of pH on the rate of curing and bioadhesive properties of dopamine functionalized poly(ethylene glycol) hydrogels, Biomacromolecules. (2014) **15** (8), 2861
- 65. Kim, M. H., Lee, J. N., Lee, J., Lee, H., Park, W. H., Enzymatically cross-linked poly(γ-glutamic acid) hydrogel with Enhanced tissue adhesive property, ACS Biomaterials Science & Engineering. (2020) 6 (5), 3103
- 66. Ercan, H., Elçin, A. E., Elçin, Y. M., Assessment of dopamine-conjugated decellularized bovine tendon extracellular matrix as a bioadhesive, Materials Today Communications. (2022) **31**, 103634
- 67. Pramudya, I., Kim, C., Chung, H., Synthesis and adhesion control of glucose-based bioadhesive via strain-promoted azide–alkyne cycloaddition, Polymer Chemistry. (2018) 9 (26), 3638

TOC

